RANS simulations for the turbulent uniform and channel flow using HDG for incompressible flow

Hashim Elzaabalawy[*,†], **Ganbo Deng**[*], **Luís Eça**[†], **and Michel Visonneau**[*]
[*]ECN/CNRS, LHEEA, Nantes/France
[†]IST, Department of Mechanical Engineering, Lisbon/Portugal
hashim.elzaabalawy@ec-nantes.fr

1 Introduction

All the industrial flow solvers dedicated to high Reynolds turbulent flows for industrial configurations are based on a formally second order accurate temporal and spatial discretization. There is a strong need for more accurate discretization approaches in many fields like computational acoustics or Large Eddy simulation which are still out of reach of systematic industrial studies. During the last ten years, several numerical methodologies have emerged, mainly for compressible flows, which look promising in terms of accuracy, computational cost and numerical robustness. A few of them concerned with incompressible flows which need very specific developments that will be the topic of this extended abstract. Numerous attempts were made to achieve high-order accurate unsteady INS solvers. However, plenty of them fails to satisfy conservation laws. Mass, momentum, and energy conservation are essential for the robustness of the method when solving the unsteady INS. Laminar flow and flows that typically have Reynolds numbers below 10^4 are not affected greatly by the lack of conservation. However, for high Reynolds numbers, i.e. turbulent flows, conservation laws must be satisfied in the numerical method to have a stable one. In order to satisfy the conservation laws numerically, the approximate velocity must be exactly divergence-free to have an energy-stable and momentum conserving method. A proposed method was developed that uses the same idea of approximation spaces mentioned in Rhebergen and Wells (2018), but with different penalization. In addition, the approximation spaces were modified so that the method can be applied for quadrilateral and hexahedral meshes.

2 Going to High-Order

It is accustomed among the CFD practitioners that high-order methods are the ones having the order of accuracy of 3 or more. The capabilities of using high-order methods are vast. Although, high-order methods can result in better accuracy, they are computationally less expensive than low-order methods. This statement is true for simple smooth problems, i.e. the Poisson equation and can easily be proven. However, is this statement true for INS on the industrial scale?
Before answering this question, the complexity added when solving the INS needs to be emphasized. The difficulty is mainly due to the incompressibility constraint and turbulence modeling. In the next section, how the high-order method can deal with the turbulent INS is briefly presented.

3 Numerical method

Hybrid Discontinuous Galerkin (HDG) provides a high-order, compact, and conservative discretization method. The hybridization offers a convenient platform to satisfy the divergence-free condition in an high-order framework, additionaly it reduces the overall operator size by reducing the number of DOF (Degrees of Freedom). However, not all HDG methods compute exact divergence-free velocity fields. Often, a post-processing operator is applied to acquire a divergence-free velocity field. Rhebergen and Wells (2018) provided a simple and efficient solution to impose the divergence-free condition using hybridization without the need of a post-processing operator to obtain an H(div)-conforming and pointwise divergence-free approximate velocity field on triangular meshes. This is achieved by carefully defining the approximation spaces of the velocity, pressure, trace velocity, and trace pressure. Most of the developed HDG methods for INS use the cell mean pressure instead of the trace pressure variable. The method has been modified so it would work with turbulent flows for quadrilateral elements. The INS equation

can be written in the conservative form as,

$$\frac{\partial \boldsymbol{u}}{\partial t} + \nabla (\boldsymbol{u} \otimes \boldsymbol{u}) = -\nabla p + \nu \nabla^2 \boldsymbol{u} + s \tag{1}$$

$$\nabla \cdot \boldsymbol{u} = 0 \tag{2}$$

Just for simplicity, we assume all Dirichlet boundary with u_D defined at the boundaries. If u_D satisfies the solvability condition, then the pressure is unique up to a constant.
The bounded domain Ω is in $\mathbb{R}^d$ with boundary $\partial\Omega = \partial\Omega_D$, $d = 1, 2,$ or 3 is the physical space dimension, and $\boldsymbol{n}$ is the outward unit normal to the boundary of Ω. The domain Ω is approximated by K number of non-overlapping elements and each element has its faces F. Introducing the broken spaces $V_h(\mathcal{T})$ and $W_h(\mathcal{T})$ associated with triangulation $\mathcal{T} = \{K\}$ in Ω which are the spaces for the approximate solution. The broken spaces $\bar{V}_h(\mathcal{F})$ and $\bar{W}_h(\mathcal{F})$ associated with faces $\mathcal{F} = \{F\}$ in $\partial\Omega$ which are the spaces for the trace variable. The approximation spaces are defined as follows,

$$V_h := \left\{ \phi_h \in [L^2(\mathcal{T})]^d \ , \ \phi_h \in [\mathcal{P}_N(K)]^d \ \forall K \in \mathcal{T} \right\}, \tag{3}$$

$$\bar{V}_h := \left\{ \bar{\phi}_h \in [L^2(\mathcal{F})]^d \ , \ \bar{\phi}_h \in [\mathcal{P}_N(F)]^d \ \forall F \in \mathcal{F} \right\}, \tag{4}$$

$$W_h := \left\{ \xi_h \in L^2(\mathcal{T}) \ , \ \xi_h \in \nabla \cdot [\mathcal{P}_N(K)]^d \ \forall K \in \mathcal{T} \right\} \tag{5}$$

$$\bar{W}_h := \left\{ \bar{\xi}_h \in L^2(\mathcal{F}) \ , \ \bar{\xi}_h \in \mathcal{P}_N(F) \ \ \forall F \in \mathcal{F} \right\}. \tag{6}$$

These are the vector spaces presented in Rhebergen and Wells (2018) with a modification for the definition of the space W_h, such that the method would be exactly point wise-divergence free for any element shape. The approximate solution and trace variables are defined as follow, $u_h \in V_h$, $\bar{u}_h \in \bar{V}_h$, $p_h \in W_h$, and $\bar{p}_h \in \bar{W}_h$.
Velocity u_h is of a degree N defined on the elements, pressure p_h is of a degree same as $\nabla \cdot u_h$ defined on the elements, trace velocity $\bar{u}_h$ components and trace pressure $\bar{p}_h$ are of a degree N defined on the facets. It can be proven that the choice of this special approximation space for p_h would automatically satisfy the divergence-free condition in the approximate spaces,

$$\nabla \cdot u_h = 0$$

As the divergence-free condition represents the pressure equation. In other words, the algorithm searches for p_h which satisfies this equation. Since the approximate spaces were designed to force $\nabla \cdot u_h \in W_h$ and $p_h \in W_h$, therefore u_h will be exactly point-wise divergence-free. With this formulation the pressure acts as a Lagrange multiplier to ensure that $\nabla \cdot u = 0$ in the approximate space. Also, the LBB condition is satisfied due to the reduced space for pressure approximation. The trace pressure $\bar{p}_h$ has a different role by acting as a Lagrange multiplier to force the normal velocity continuity at the faces, $u_h \cdot n = \bar{u}_h \cdot n$. These two conditions can be written as,

$$\int_K u_h \cdot \nabla \xi_h \, dx - \int_{\partial K} u_h \cdot n \xi_h \, ds = 0 \quad \forall \xi_h \in W_h, \tag{7}$$

$$\int_{\partial K} u_h \cdot n \bar{\xi}_h \, ds - \int_{\partial K} \bar{u}_h \cdot n \bar{\xi}_h \, ds = 0 \quad \forall \bar{\xi}_h \in \bar{W}_h, \tag{8}$$

After satisfying the mass continuity, a new variable $\boldsymbol{q}$ is defined to make the diffusion term suitable for HDG,

$$\frac{\partial \boldsymbol{u}}{\partial t} + \nabla \boldsymbol{f} = -\nabla p + \nu \nabla \boldsymbol{q} + s \tag{9}$$

$$\boldsymbol{q} - \nabla \boldsymbol{u} = 0 \tag{10}$$

$$\boldsymbol{f} = \boldsymbol{u} \otimes \boldsymbol{u} \tag{11}$$

In which the trace variable $\bar{q}_h$ is defined in terms of the velocity as,

$$n \cdot (\bar{q}_h - q_h) = \tau (\bar{u}_h - u_h) \tag{12}$$

where τ is a penalty parameter to ensure stability. For the sake of brevity, HDG discretization is applied on the viscous, pressure, and advection terms to reach the final discretized form.

4 Turbulence Model

Another challenge that faces the high-order accurate INS is the turbulence modeling. For industrial applications at high Reynolds numbers, RANS is the most convenient method to simulate turbulence in terms of computational time. Unfortunately, RANS has the largest modeling error. Hybrid LES/RANS provides a solution that compromises between computational time and modeling accuracy, but yet involves RANS modeling. It can be agreed upon that RANS is indispensable in the meantime for industrial applications. For that reason, the high-order accurate INS solver needs to be capable of solving the RANS equations. To solve the linear eddy viscosity RANS, a turbulence model is required to acquire the eddy viscosity. The $k-\omega$ model includes two convection-diffusion equations with source terms. However, they form a stiff operator due to their non-linearity. Furthermore, the k profile near the wall has very high gradients and ω goes to infinity at the wall, this adds more complexity. Due to the non-linearity and the huge gradients, oscillations appear near the high gradient zone. These oscillations result in negative quantities for k and ω. Physically, these quantities can never be negative. With the change of sign, production and dissipation terms are reversed, thus leading to a solution blowup. What even makes this worse is that oscillations increase as Reynolds numbers increase or as the polynomial order increases. Which makes high Reynolds number flows very challenging to model with high-order methods. Nonetheless, in this extended abstract attempts were made to solve the turbulence equations using HDG. There are different types of $k-\omega$ models, and the Wilcox 1998 model is chosen to start with.

5 Uniform flow test case

Although the uniform flow test case is a simple test, it can be a useful test case to check the divergence-free condition. Additionally, the turbulence model can be tested, as the analytical solution is expressed by Spalart and Rumsey (2007). The computational domain is a rectangle and inlet velocity is applied from the left boundary, which is equal to 1 in the x-direction and 0 in the y-direction. Symmetry boundary condition is applied at the bottom edge and outflow at the right and top edges. First, to show the importance of using divergence-free methods, the conventional HDG is compared with the developed point-wise divergence-free HDG for quadrilaterals. The contour of the divergence of velocity is plotted for the two methods at different viscosities using 4^{th} order HDG. These results were plotted after 6 linear iterations for the steady state INS.

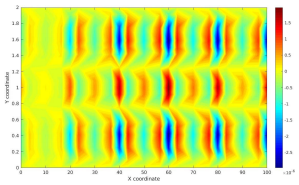

Fig. 1: $\nu = 10^{-2}$

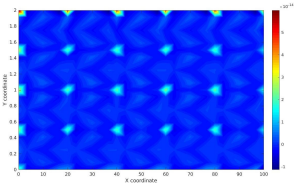

Fig. 2: Div-free $\nu = 10^{-2}$

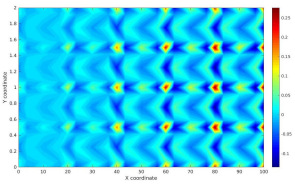

Fig. 3: $\nu = 10^{-9}$

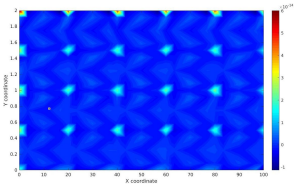

Fig. 4: Div-free $\nu = 10^{-9}$

It can be clearly seen that divergence increases as viscosity decreases in the conventional HDG method. While the point-wise divergence-free HDG always maintains a divergence-free velocity field upto the machine precision for any viscosity. In the steady case for low Reynolds numbers, this divergence in the velocity can be somehow accepted, however in transient cases the blow up is definite for long duration simulations. The divergence-free HDG is then coupled with the $k-\omega$ turbulence model. The values of k and ω are specified at the inlet. It is expected to for the turbulence variables to decay in the x-direction. The results obtained are plotted for $\nu = 10^{-6}$ at different and polynomials degrees and stretching near the inlet using quad meshes.

The polynomial degree of 2, 4, 6, and 10 with 23, 24, 21, and 22 DOF respectively in the x-direction are used. In the first case, the stretching was not enough to obtain stable solutions for higher order cases as shown in Fig. 5. While for the larger stretching, the results were stable even for the 10^{th} order approximation. For equally spaced elements in x, only the 2^{nd} order was stable, and the solution exhibits an undershoot that gives negative turbulence values. Apart from the shortcomings regarding stability, the

accuracy increases as the order increases as it can be shown in the Fig. 5,6,7. An important finding from these results is that, order-refinement increases the accuracy but upto a certain limit then it results in negative turbulence quantities then it blows up.

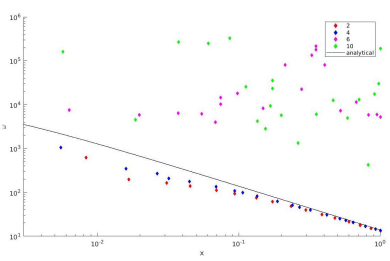

Fig. 5: ω on a less stretched mesh

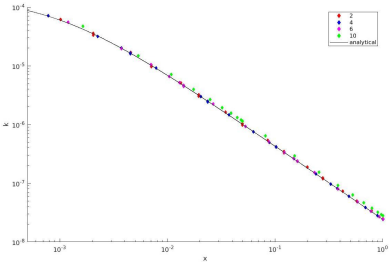

Fig. 6: k on a stretched mesh

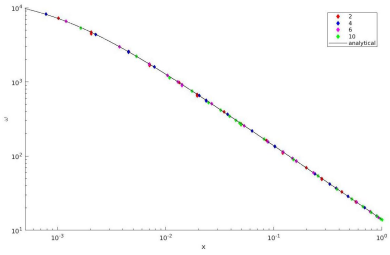

Fig. 7: ω on a stretched mesh

6 Channel flow test case

To understand the behavior of high-order RANS near the boundary layer in fully turbulent flows, the channel flow test case is chosen. Periodic boundary conditions are applied in the flow direction for all the variables, while no-slip wall boundary condition is applied on the other direction. A constant source term is added to the momentum equation as a pressure gradient to induce a flow. By keeping the source term as a constant, various mesh sizes are used for code verification.
The solutions are compared to the classical finite volume solution, where $y+$ and the DOF are kept the same. The solution of the finite volume on a very fine grid is used as a reference solution to compare the FV and 3$^{\text{rd}}$ order HDG. Tests were made at $Re = 2 \times 10^6$ with 40, 60, and 120 DOF in the y-direction. The corresponding $y+$ is 1.6, 0.85, and 0.36 respectively. While the second nearest element to the wall is located at $y_{elem}+$ of 5.7, 3.1, and 1.3 respectively. The near wall analytical solution for ω is used as a boundary condition for the second nearest element to the wall,

$$\omega = \frac{6\nu}{\beta_o y_{wall}^2} \quad \text{as} \quad y_{wall} \to 0 \tag{13}$$

Results are shown for the lower half of the channel with a half-height of 1 using structured triangular meshes. The value of the penalty parameters τ, τ_k, and τ_ω are set to $\frac{Re}{200}$.
It can be seen that HDG predicts better profiles for the velocity, k, and ω near the wall. However, the values of k at the channel centerline are always less than the FV and the reference solution. At the very coarse mesh in Fig. 12 the oscillations near the curve maximum is visible. In Fig. 11, HDG gives a much better result than the FV for the whole velocity profile. It is observed that lower $y+$ values are needed as the Reynolds number increases. The observations were nearly the same for higher Reynolds number. An overshoot of k near the maximum value is also noticed in Fig. 12. It is noted that the reference values is only considered as the best possible result for FV at finner meshes not the overall best results. In addition, the HDG solution does not match the FV solution on the very fine mesh as shown in Fig. 20-22.

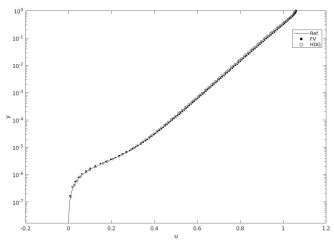

Fig. 8: u at $Re = 2 \times 10^8$ with 120 DOFs at $y+ = 0.29$

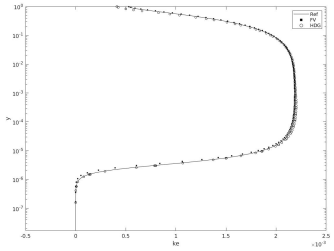

Fig. 9: k at $Re = 2 \times 10^8$ with 120 DOFs at $y+ = 0.29$

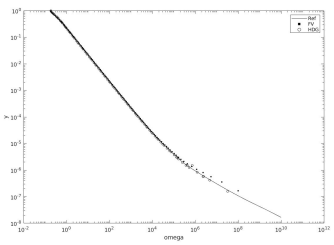

Fig. 10: ω at $Re = 2 \times 10^8$ with 120 DOFs at $y+ = 0.29$

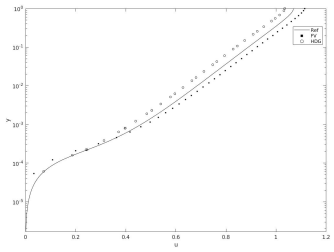

Fig. 11: u at $Re = 2\times10^6$ with 40 DOFs at $y+ = 1.6$

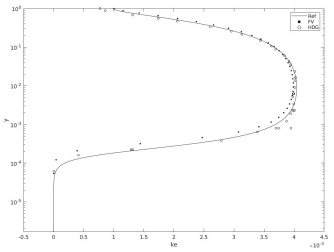

Fig. 12: k at $Re = 2\times10^6$ with 40 DOFs at $y+ = 1.6$

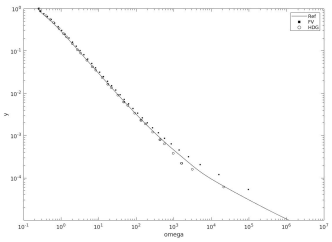

Fig. 13: ω at $Re = 2\times10^6$ 40 120 DOFs at $y+ = 1.6$

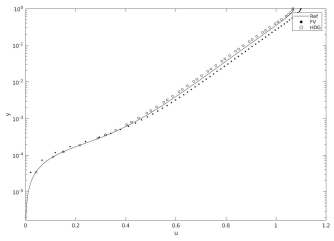

Fig. 14: u at $Re = 2\times10^6$ with 60 DOFs at $y+ = 0.85$

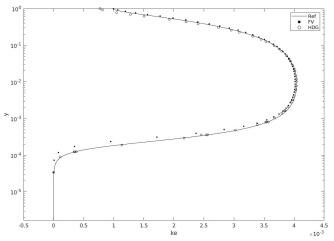

Fig. 15: k at $Re = 2\times10^6$ with 60 DOFs at $y+ = 0.85$

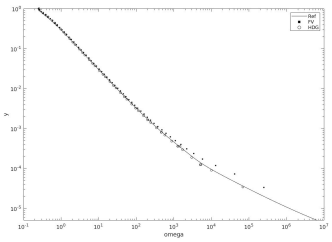

Fig. 16: ω at $Re = 2\times10^6$ with 60 DOFs at $y+ = 0.85$

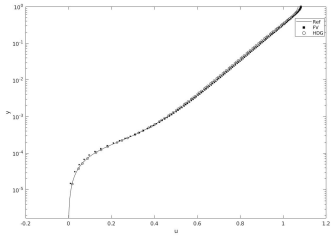

Fig. 17: u at $Re = 2\times10^6$ with 120 DOFs at $y+ = 0.36$

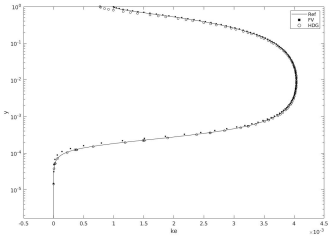

Fig. 18: k at $Re = 2\times10^6$ with 120 DOFs at $y+ = 0.36$

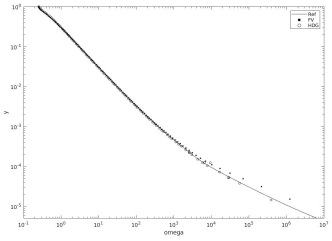

Fig. 19: ω at $Re = 2\times10^6$ with 120 DOFs at $y+ = 0.36$

For the velocity, there is a considerable difference between the FV and DG solutions in the velocity near the centerline of the channel. A similar difference is observed in Fig. 21 for k. While the largest difference in ω is near the wall as shown in Fig 22. At the moment, the exact reason why the FV solution does not match the DG solution at the very fine is not clear. Nevertheless, it is suggested that this mismatch is due to the different treatment of the boundary condition for ω at the wall.

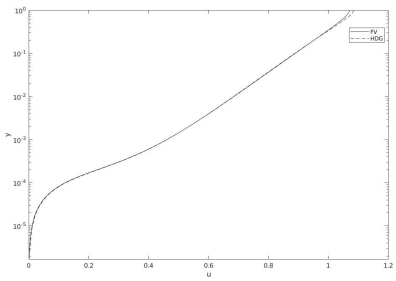

Fig. 20: u plot for HDG vs FV on a very fine grid at $Re = 2\times10^6$

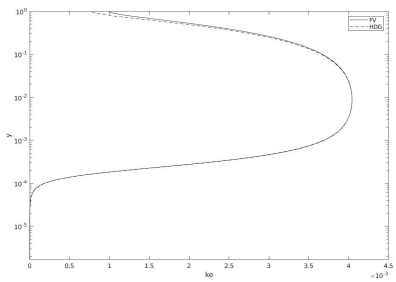

Fig. 21: k plot for HDG vs FV on a very fine grid at $Re = 2\times10^6$

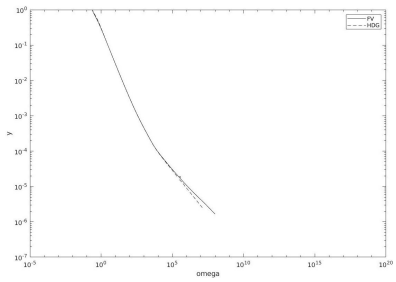

Fig. 22: ω plot for HDG vs FV on a very fine grid at $Re = 2\times10^6$

At this range of high Reynolds numbers, verification exercise is more useful than validation for such test case. The velocity and turbulence quantities are computed at different meshes to perform a grid re-

finement study. Then the results are fitted to a power series in order to estimate the convergence rate. The number of elements in y changed from 30 to 300, this corresponds to $y+$ values of 0.85 to 0.10 and $y_{elem}+$ values of 3.1 to 0.37 respectively. The mean and maximum velocity, maximum k, min ω, and shear stress at the wall are chosen to estimate their convergence rates. Expected convergence rates were obtained which is roughly equal $N+1$ for all variables except the shear stress. The shear stress convergence is not monotonic, possibly due to the near wall oscillations for the mesh with 30 elements in y.
Negative values of k are observed near the wall with some oscillations, however as these values are restricted to the viscous sublayer, their effect are negligible. Unfortunately, if these negitive values appeared in the rest of the domain, they obstruct the convergence. To solve this problem, a generalization of limiting negative k values to zeros and taking the absolute values of ω is proposed to fit the high-order method. During the simulation it was noticed that, as long as the the cell averaged values of the turbulence quantities are positive, the convergence can be guaranteed. Thus, a scaling limiter is applied to preserve the value of the cell average of the element with eliminating the negative values. The scaling limiter is defined in the paper by Zhang and Shu (2010), is applied to limit k and $\frac{1}{\omega}$.

7 Conclusion

The challenges of achieving an industrial high-order incompressible RANS $k-\omega$ solver can be clarified in this report. Fundamentally, an algorithm which is capable of calculating a point-wise exactly divergence-free velocity that can be used for hexahedral and tetrahedral is essential. The method presented in this report has this feature without the need of post-prepossessing operators or unclear penalization. However, the reduced element proposed needs to be optimized. In addition, a study on improving the penalty parameter would be useful at high Reynolds numbers as increasing the penalty parameter for the whole domain increases the conditioning number of the global matrix. Moreover, the global operator lost its symmetry with the introduction of turbulence. For that reason, efficient preconditioners are strongly required for these kinds of problems in order to compete with the finite volume solvers. The channel flow test case gives an indication that high-order RANS solvers have the ability to outperform the finite volume solvers in terms of accuracy per degrees of freedom. Yet, the computational time would be less for the finite volume solvers for the current implementations.

With the introduction of the scaling limiter, the $k-\omega$ equations can be solved using high-order methods. Nevertheless, it is not clear what should be done if the average mean values of the turbulence quantities fail to have positive values. The implicit treatment of the negative source terms may solve this problem. In order to fully test this method, test cases other the 2D channel and uniform flow should be used.

High-order RANS for INS is promising and with some more adjustments, high-order INS solvers can compete with the FV solvers in terms of robustness.

Acknowledgements

This work is done with the funding of SEED Erasmus Mundus Joint Doctorate. We thank Sonia Fernández-Méndez and Jeroen Wackers for their efforts and recommendations.

References

Rhebergen, S., & Wells, G. N. (2018). A hybridizable discontinuous Galerkin method for the Navier?Stokes equations with pointwise divergence-free velocity field. Journal of Scientific Computing, 76(3), 1484-1501.

Wilcox, D. C. (1998). Turbulence modeling for CFD (Vol. 2, pp. 172-180). La Canada, CA: DCW industries.

Spalart, P. R., & Rumsey, C. L. (2007). Effective inflow conditions for turbulence models in aerodynamic calculations. AIAA journal, 45(10), 2544-2553.

Zhang, X., & Shu, C. W. (2010). On maximum-principle-satisfying high order schemes for scalar conservation laws. Journal of Computational Physics, 229(9), 3091-3120.